International Journal of Nanomedicine

Dovepress
Taylor & Francis Group

Open Access Full Text Article

ORIGINAL RESEARCH

Dissolvable Microneedle Administration Combined with Ultrasonic Cavitation Promotes Melanoma Penetrating Capability of Ce6

Binrui Shi[1–5,*], Mingjie Li[1–5,*], Renjie Feng[1–5], Guihua Wang[6], Liyong Deng[6], Yueyong Li[6], Kezhen Wang[1–3,7], Meng Du[1–3,5], Zhiyi Chen[1–3,5]

[1]Key Laboratory of Medical Imaging Precision Theranostics and Radiation Protection, College of Hunan Province, the Affiliated Changsha Central Hospital, Hengyang Medical School, University of South China, Changsha, Hunan, 410004, People's Republic of China; [2]Institute of Medical Imaging, Hengyang Medical School, University of South China, Hengyang, Hunan, 421001, People's Republic of China; [3]Department of Medical Imaging, The Affiliated Changsha Central Hospital, Hengyang Medical School, University of South China, Changsha, Hunan, 410004, People's Republic of China; [4]The Seventh Affiliated Hospital, Hunan Veterans Administration Hospital, Hengyang Medical School, University of South China, Changsha, Hunan, 410118, People's Republic of China; [5]Institute for Future Sciences, University of South China, Changsha, Hunan, 410008, People's Republic of China; [6]Department of Oncology, the Affiliated Changsha Central Hospital, Hengyang Medical School, University of South China, Changsha, Hunan, 410004, People's Republic of China; [7]College of Mechanical Engineering, University of South China, Changsha, Hunan, 410004, People's Republic of China

*These authors contributed equally to this work

Correspondence: Meng Du; Zhiyi Chen, Key Laboratory of Medical Imaging Precision Theranostics and Radiation Protection, College of Hunan Province, the Affiliated Changsha Central Hospital, Hengyang Medical School, University of South China, Changsha, Hunan, 410004, People's Republic of China, Email dumeng_work@126.com; zhiyi_chen@usc.edu.cn

Purpose: Melanoma, a highly aggressive superficial malignancy with rising incidence and mortality, faces limited sonodynamic therapy (SDT) efficacy due to poor sonosensitizer accumulation and penetration. To overcome this, we employed chlorin e6 (Ce6), a high-ROS-yield sonosensitizer, and enhanced its tumor delivery using a synergistic microneedle (MN) and ultrasound (US) strategy.

Methods: Using melanoma as an application scenario, a "stepwise drug delivery" system was developed. It consisted of dissolving MN encapsulating US-responsive nanoparticles (Ce6-PFP@PLGA, CPP) and termed CPP@MN. CPP@MN breaks through the stratum corneum to deliver CPP to tumors, followed by US-triggered cavitation that mediates perfluoropentane (PFP) phase transition to enhance the tumor-penetrating capability of chlorin e6 (Ce6). Delivery efficacy was validated using three experimental models: an in vitro agarose skin phantom, ex vivo pig skin, and in vivo tumors. Furthermore, the anti-tumor efficacy of US-combined CPP@MN was evaluated at the cellular level and in tumor-bearing mice.

Results: According to the results, CPP@MN showed excellent transdermal performance, including rapid dissolution of sonosensitizer and sufficient mechanical strength. MN combined with US increased the tumor penetration depth of loading drug by 2.5–4 times across all experimental models. Ultrasonic cavitation promotes nanoparticle-derived Ce6 release and deeper tumor diffusion, resulting in specific anti-tumor efficacy.

Conclusion: This innovative "stepwise drug delivery" system addresses persistent challenges in superficial tumor SDT, including inadequate sonosensitizer aggregation and poor tissue penetration, while establishing a multifunctional platform for spatiotemporally controlled drug release that sequentially overcomes the skin biological barriers.

Keywords: transdermal drug delivery, microneedle, ultrasonic cavitation, superficial tumors, sonodynamic therapy

Introduction

The unique appearance—including color, shape, and location—of superficial skin tumors (SSTs), such as breast cancer, basal or squamous cell carcinoma, head and neck cancer, human oral epidermoid carcinoma, and melanoma, causes considerable physical and psychological distress for patients.[1] Melanoma is one of the most aggressive human malignancies, with around 288,000 patients diagnosed and 61,000 patients died each year worldwide according to cancer statistics 2022.[2] Sonodynamic therapy (SDT), which mainly involves the activation of sonosensitizers using ultrasound

Received: 15 May 2025
Accepted: 10 October 2025
Published: 30 October 2025

(US) to produce reactive oxygen species (ROS),[3] has shown excellent clinical potential and transformation value in the field of superficial tumor treatment,[4] with the advantage of low systemic toxicity. Therefore, sufficient accumulation of the sonosensitizer in tumor tissue is the key to the high effectiveness of SDT.[5] As for superficial tumor, conventional drug delivery routes (eg, intravenous injection, oral administration) often result in suboptimal tumor-specific accumulation and non-targeted organ distribution, significantly limiting therapeutic efficacy, with potential concerns of systemic toxicity.[6] While percutaneous local injection carries inherent risks of infection, hemorrhage, and tissue trauma,[7] chronic subcutaneous administration additionally generates substantial biomedical waste.[8] Therefore, it is urgent to explore an ideal drug delivery system for superficial tumor.

Currently, transdermal drug delivery strategies have received extensive attention in the field of superficial tumors treatment.[9] The Transdermal Drug Delivery System (TDDS) enables drugs to penetrate the skin's stratum corneum, reach the dermis, enter the bloodstream through capillaries, and ultimately target the diseased area via systemic circulation. This unique drug delivery method avoids the liver first-pass effect as well as the destruction of drugs in the gastrointestinal tract.[10] The most widely accepted TDDS is microneedle (MNs) based drug delivery, which employs arrays of micron-sized needles to penetrate the skin surface in a minimally invasive manner. This technique achieves local disruption of the skin barrier and shedding of the stratum corneum, thereby creating microchannels for drug delivery. By enabling efficient transdermal drug permeation, it significantly reduces the required dosage and drug concentration compared with conventional methods.[7,11] Thus, MNs have the advantages of intense stratum corneum penetration capability, good biocompatibility, and high safety, making them suitable for superficial tumor treatment.[1]

Although microneedles have achieved the purpose of minimally invasive drug delivery owing to their unique advantages, limited penetration depth of drugs carried (200–1000 μm)[7] and lack of active regulation of the delivery process are the main bottlenecks of MN-based drug delivery methods.[12] Various strategies have been explored to enhance drug penetration depth, including penetration enhancers, iontophoresis, laser/magnetic/thermal stimulation, electroporation, and nanocarriers.[13] However, the delivery efficiency of thermal stimulation and electroporation is limited by its side effects, such as invasiveness and safety concerns,[14] while the devices needed for magnetic stimulation are often expensive, complex, and poorly adaptable to diverse environments.[15] Excessive chemical modifications of nanoparticles increase the risk of systemic toxicity, particularly when targeting long-term biocompatibility.[16] Therefore, the current application status of MNs underscores the critical demand for microneedle-assisted delivery systems to overcome skin barriers and enhance the spatiotemporal control of depth penetration of drugs.

US has emerged as a promising solution for drug/gene delivery,[17–19] offering deep-tissue penetration and spatiotemporally controlled capabilities. US-mediated penetration has been demonstrated to achieve depths exceeding 5 cm, crossing the skin and connective tissues,[20,21] enabling spatiotemporally controlled drug release at deep site.[22] The mode of US-triggered drug release primarily via cavitation, mechanical forces, and localized heating, which enhances the concentration of drugs in the microenvironment and transiently permeabilizes cell membranes, facilitating intracellular drug influx.[23] In addition, the porphyrin derivative chlorin e6 (Ce6) is a second-generation sensitizer with potent acoustic activity.[24] Basic research revealed that Ce6 produces higher levels of singlet oxygen, has a shorter skin retention time, a higher clearance rate, and fewer side effects. Following the development of sonodynamic therapy (SDT), the role of Ce6 in ultrasound therapy was extensively researched.[25]

In summary, in order to enhance the tumor-penetrating capability of sonosensitizers in superficial tumors, we build a "stepwise drug delivery" system integrating dissolvable microneedles with US-responsive nanoparticles (Figure 1). This system operates through two sequential phases: (1) controlled initial penetration: upon skin insertion, CPP@MN dissolves to release nanoparticles, enabling localized sonosensitizer deposition within the tumor tissue; and (2) US-triggered deep penetration capability, which activates PFP-generated microbubbles, inducing cavitation effects to simultaneously liberate sonosensitizers from nanoparticles and propel microneedle-tip-loaded agents across the dermal barrier into deeper tumor regions, thereby amplifying therapeutic efficacy. By synergizing microneedle transdermal drug delivery combined with ultrasonic cavitation, this strategy overcomes the critical limitations of conventional SDT, including sonosensitizer aggregation and restricted tissue penetration, while offering a versatile and minimally invasive approach for precise tumor targeting. Our findings highlight the potential of this drug delivery system as a translatable paradigm for superficial tumors.

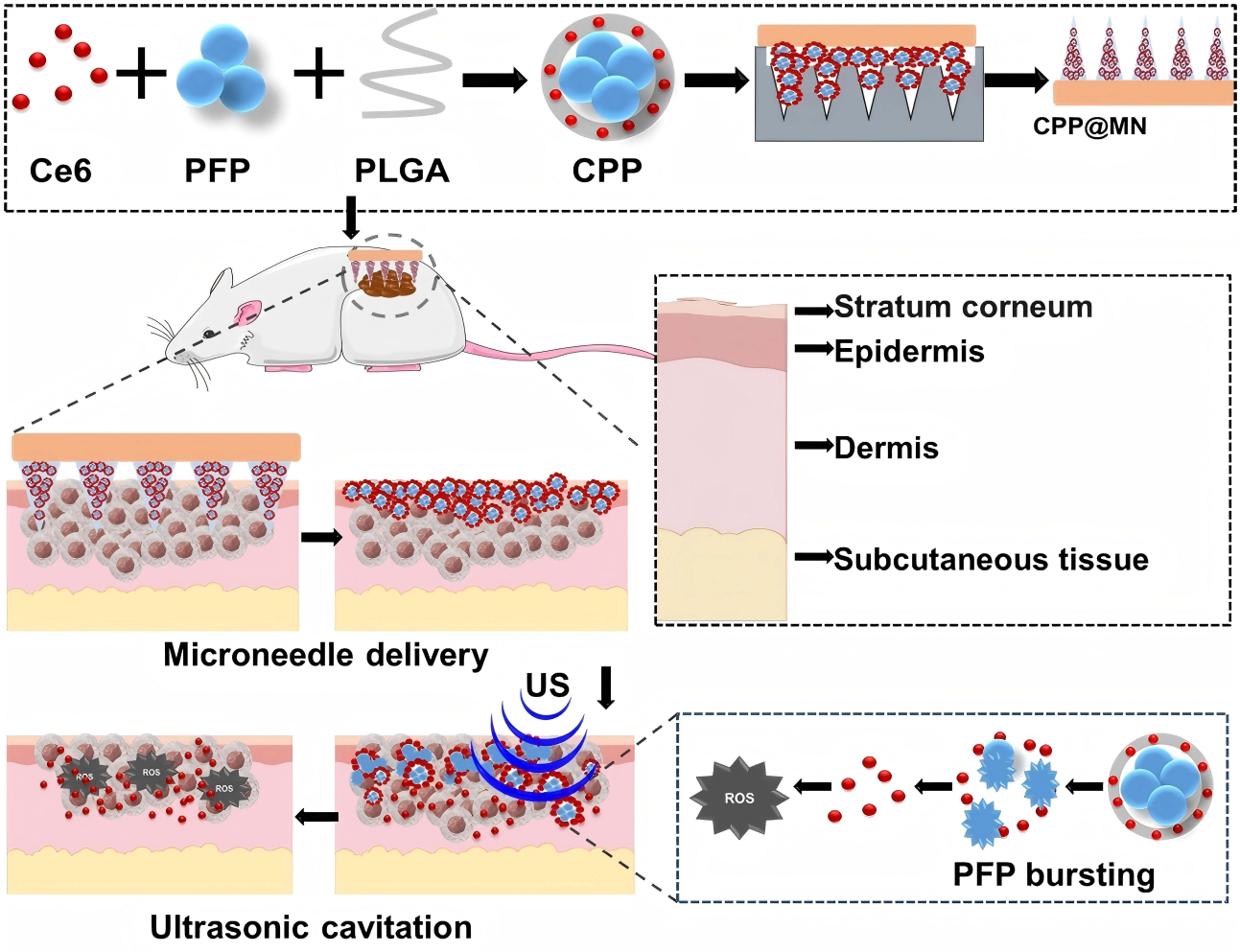

Figure 1 Schematic illustration of CPP@MN combined with US promoting drug permeation-mediated tumor SDT.

Materials and Methods

Material

Poly (lactic-co-glycolic acid) (PLGA; 50:50, 5 kDa, COOH-terminated) was obtained from Risi (Xi'an, China). Perfluoropentane (PFP) and chlorin e6 (Ce6) were purchased from Aladdin (Shanghai, China). Dimethyl sulfoxide (DMSO), hyaluronic acid (HA), and Evans Blue were acquired from Seguin (Shanghai, China), Yi Reagent (Shanghai, China), and Sijia (Guangzhou, China), respectively. Poly (vinyl alcohol) (PVA) 1788; 87.0–89.0% (mol/mol) and PVP; 9003–39-8; K-17 were obtained from yuanye (Shanghai, China). MES buffer, pH 7.0 (MES) and agarose were supplied by Unk Times (Beijing, China) and McLean (Shanghai, China), respectively. The (PDMS) precursor was procured from the Dow Corning Corporation (Midland, MI, USA). The lipophilic fluorescent dye, 3,3'-dioctadecyloxacarbocyanine perchlorate (DiO), was obtained from Bairuiji (Anhui, China). The B16F10 cells were purchased from SUNNCELL (Shanghai, China). The freshly isolated abdominal pig skin (commercially purchased) was used as the ex vivo skin model.

Preparation and Characterization of CPP

CPP nanoparticles were synthesized using a double-emulsion method. The oil phase comprised PLGA (40 mg), Ce6 (2 mg), DMSO (100 μL), and dichloromethane (2 mL). After the addition of 4% (w/v) Polyvinyl alcohol (PVA) and 200 μL of PFP, the mixture was sonicated twice. The suspension was then treated with 10 mL of 2% (v/v) isopropanol and stirred at 25°C for 4 h to evaporate dichloromethane, yielding CPP.

https://doi.org/10.2147/IJN.S537983

The preparation of PFP@PLGA (PP) was the same as that of CPP except that Ce6 was not added. DPP and EPP were prepared similarly, with Ce6 replaced by DiO or Evans Blue, respectively.

The loading efficiency of Ce6 was verified by comparing the ultraviolet-visible (Vis) absorption spectra of CPP, PP, and free Ce6. Subsequently, 50 μL of freshly prepared CPP solution was diluted to a final volume of 1 mL with purified water and the size was characterized using a dynamic light scattering (DLS) instrument (Micromeritics, USA).

Evaluation of Drug Release Capacity of CPP in vitro

A Sonovitro ultrasonic irradiator instrument (ShengXiang, China) was used for US irradiated: CPP solutions was dispersed in the MES buffer, with various US irradiated duration (20, 60, 180, 300 s) and acoustic pressure (0.6, 1.2, 1.8, 2.4 W/cm²), and us parameters was fixed (1 MHz, 50% duty cycle). After US irradiation, the CPP solutions were collected and centrifuged (10,500 rpm, 10 min), and the optical intensity at 403 nm (the peak intensity of Ce6) was measured using a UV-VIS spectrophotometer. The cumulative release concentration was calculated using the Ce6 standard curve and was represented as the release amount (%).

$$\text{Release amount (\%)} = (Mt/M\infty) \times 100$$

Mt represents the cumulative amount of Ce6 released from the CPP after US irradiation and M∞ is the total amount of Ce6 contained in the CPP.

US images of CPP irradiated using US irradiation (1.2 W/cm^2, 1 MHz) for different durations were acquired synchronously.

Preparation of CPP@MN

CPP@MNs were prepared using a two-step micro-molding protocol. First, a precursor solution containing CPP and 20% hyaluronic acid (HA) was infused into a polydimethylsiloxane (PDMS) mold under vacuum-assisted conditions (−0.08 MPa, 25 min), followed by removal of excess material and air-drying at 25°C for 2 h. Subsequently, a backing layer solution composed of 20% polyvinyl alcohol (PVA) and 50% polyvinylpyrrolidone (PVP) was introduced into the mold under reduced pressure (−0.05 MPa, 5 min). The composite structure was thermally cured overnight at 25°C, demolded from PDMS, and stored in a desiccator under ambient conditions.

DPP@MNs and EPP@MNs were prepared similarly, with CPP replaced by DPP or EPP.

Evaluation of CPP@MN Solubility

Freshly isolated pig skin was removed and disinfected via shaving. CPP@MN was vertically inserted into the skin and removed after 1, 5, 10, 15, and 20 min. The height of the needle tip was observed immediately using a stereomicroscope (Laite, Guangzhou, China).

Mechanical Strength Test of CPP@MN

CPP@MN was fixed to a horizontal platform with the tip facing straight up. Place a flat-bottomed container (1000 mg) on top of the needle tip, gradually add round beads (200 mg each) to the container, and observe the changes in the needle tip in real time using a stereomicroscope. Record the compression distance of the CPP@MN tip under different weights (number of beads × 200 mg+1000 mg). Finally, the weight is converted to Newtonian force (1N=0.1kg), and the compression curves of CPP@MNs are prepared under different forces.

Cell Culture

B16F10 cells were cultured in Dulbecco's modified Eagle medium (DMEM) containing 10% heat-inactivated fetal bovine serum (FBS) and 1% penicillin and streptomycin (P/S). Cells were incubated at 37°C in a 5% CO_2 atmosphere.

Animal

Female Balb/c mice (18–20 g) were obtained from Silek Jingda Laboratory Animal Co., Ltd. (Hunan, China). Tumor-bearing models were established by the subcutaneous administration of B16F10 cells (100 μL suspension containing 1×10^6 cells/mL) into the right abdominal region. Seven days after cell inoculation for 7 days, mice that successfully developed melanoma lesions were randomized into experimental groups for therapeutic interventions.

All procedures were conducted in accordance with ethical guidelines approved by the Institutional Animal Care and Use Committee of the Hunan Prevention and Treatment Institute for Occupational Diseases, affiliated with the University of South China (Ethics Approval No. HNZFY-FE-0301).

Skin Penetration Capability Verification of MN

To visually display the skin penetration ability of CPP@MN, Evans Blue dye was used as a model drug instead of Ce6. The EPP@MN was vertically inserted into isolated pig skin and removed after continuous thumb pressure for 20 min. A porous structure was observed on the skin surface.

Evaluation of MN-Mediated Drug Delivery Enhancement Combined with Ultrasonic Cavitation in vitro

Agarose skin phantom construction: Agarose was dissolved in purified water, prepared into a 0.026 g/mL solution, poured into a mold after microwave heating, and then left to cool and solidify at room temperature. EPP@MN was inserted into the agarose skin phantom and irradiated in different groups: the experimental group was irradiated by US, whereas the control group was not irradiated by US. After treatment, the penetration depth of the model in Evans Blue was observed using a stereomicroscope and quantitative analysis was performed.

DPP@MN was vertically inserted into isolated pig skin (2 × 2 cm) and then removed after continuous thumb pressure for 20 min. The experiment was divided into four groups: (1) DPP@MN combined with US irradiation (DPP@MN+US), (2) DPP@MN without US irradiation, (3) subcutaneous injection of DPP (DPP-i.H), and (4) subcutaneous injection of DPP combined with US irradiation (DPP-i.H+US). After treatment, isolated pig skin tissues were frozen, the green fluorescence distribution of DiO was observed by fluorescence microscopy, and the penetration depth of DiO was quantitatively analyzed.

(US: 1 MHz, 1.4 W/cm², 20% duty cycle, 5 min)

Evaluation of MN-Mediated Drug Delivery Enhancement Combined with Ultrasonic Cavitation in vivo

The therapeutic procedure was as follows: CPP@MN was administered intratumorally and removed immediately 2 min after application. Skin recovery kinetics were monitored to assess the minimally invasive nature of the intervention. The mice were then immobilized in the supine position, and DPP@MN was positioned over the tumor with uniform pressure applied for 20 min to ensure full tumor coverage. Animals were randomly allocated to US irradiation or untreated control groups. At 0.5 h post-intervention, tumor tissues were harvested, snap-frozen, and sectioned for fluorescence microscopy analysis to evaluate the distribution and penetration efficiency of DiO-labeled nanoparticles.

(US: 1 MHz, 1.4 W/cm², 20% duty cycle, 5 min)

Cell Uptake Assay

B16F10 cells were seeded at a density of 1×10^5 per well in 24-well plates and incubated at 37°C in a 5% CO_2 incubator for 24 h. Subsequently, the medium was replaced with fresh medium containing DPP and microneedle tips. The cells were then cultured in this mixture. After 0, 2, 4, and 8 hours, cells were washed with PBS and stained with DAPI.

In vitro Cytotoxicity Verification and Sonodynamic Effect Detection of CPP

B16F10 cells were seeded in 96-well plates (1×10^4 cells/well) and incubated at 37°C/5% CO_2 for 24 h. Fresh medium containing varying concentrations of CPP was added to each well and co-incubated with cells. After 4 h, cells were

washed with PBS, replenished with fresh medium, and either sonicated or left untreated. A fresh medium: CCK-8 mixture (9:1) was prepared in advance. After 40 min, this mixture was added to all wells (including blanks containing medium only). Plates were gently shaken to mix, avoiding bubbles, and returned to the incubator. Absorbance at 450 nm was measured after observable color development.

$$\text{Cell Viability} = [\,(\text{As} - \text{Ab})/\,(\text{Ac} - \text{Ab})\,] \times 100\%$$

Cellular ROS Detection

B16F10 cells (5×10^4 cells/well) were seeded into 24-well plates, cultured for 12 h, and treated as follows: (1) control, (2) US, (3) CPP, (4) CPP+US, (5) CPP@MN, and (6) CPP@MN+US. DCFH-DA was added, and the cells were incubated for 30 min in the dark. After washing with PBS, the fluorescence intensity of the ROS was measured and quantitatively analyzed. (US: 1.0MH, 1.2 W/cm^2, 1min, 50% duty cycle)

Live/Dead Cell Staining

B16F10 cells (5×10^4 / well) were seeded in 24-well plates and incubated at 37°C. After different treatments, the cells were stained with calcein-AM and PI for 20 min to distinguish between living and dead cells after rinsing with PBS. Finally, stained cells were observed under a fluorescence microscope. (US: 1.0MH, 1.2 W/cm^2, 1min, 50% duty cycle)

Anti-Tumor Effects in vivo

Female BALB/c mice (6–8 weeks old) were subcutaneously injected with B16F10 cell suspensions (1×10^6 cells/mL, 100 μL) in the right abdominal region. One week post-inoculation, tumor-bearing mice were randomly divided into four treatment groups (n=4): (1) control, (2) CPP@MN, and (3) subcutaneous injection combined with US irradiation (CPP- i. H + US); and (4) CPP@MN+US.

For groups 2 and 4, CPP@MN patches were implanted intratumorally for 5 min. US irradiation (1 MHz, 1.4 W/cm², 50% duty cycle, 5 min) was initiated 20 min post-implantation for the designated groups. All intervention measures were performed every three days. The size of the tumor was measured with a caliper every two days, and the volume was calculated as $V = L \times W^2/2$. Terminal tumors were excised after euthanasia for histopathological analysis (H&E staining) and apoptosis assessment (TUNEL assay).

Statistical Analysis

All data were collected from three independent experiments (triplicate samples per condition) and are expressed as the mean ± SD. Two-way ANOVA and Student's *t*-test were used for significance analysis (*$p < 0.05$, **$p < 0.01$, ***$p < 0.001$, and ****$p < 0.0001$). All analyses were performed using GraphPad Prism version 8.

Results

Characterization of the CPP and CPP@MN

Ce6-PFP@PLGA nanoparticles (CPP) were prepared using the double-emulsion method. UV-VIS absorption spectra showed that CPP exhibited a characteristic Ce6 peak at 403 nm (Figure 2a). The dynamic light scattering method characterized the nanoparticles before and after Ce6 loading: the particle size of blank carrier PP was 164.2 ± 3.5 nm, and the particle size of drug-carrying nanoparticle CPP was 190.1 ± 4.2 nm. The particle size distributions of both nanoparticles showed a unimodal normal distribution, and the particle size increased by approximately 15.8% after loading, indicating that the loading of Ce6 did not significantly change the size characteristics of the nanoparticles (Figure 2b). The effective release of drugs after US irradiation was key to this study. CPP was irradiated using different US parameters. The results showed that, under a fixed parameter (1 MHz, 50% duty cycle), the release amount increased with an increase in the irradiation time (34.84% for 5 min) at 0.6 W/cm². At 1.2 W/cm², the release amount reached 43.08 ± 10.85% in 3 min. When the intensity was greater than 1.2 W/cm² and the US irradiation time exceeded 1 min, the release curve exhibited a downward trend (Figure 2c). As shown in Figure 2d, US-induced grayscale variations were

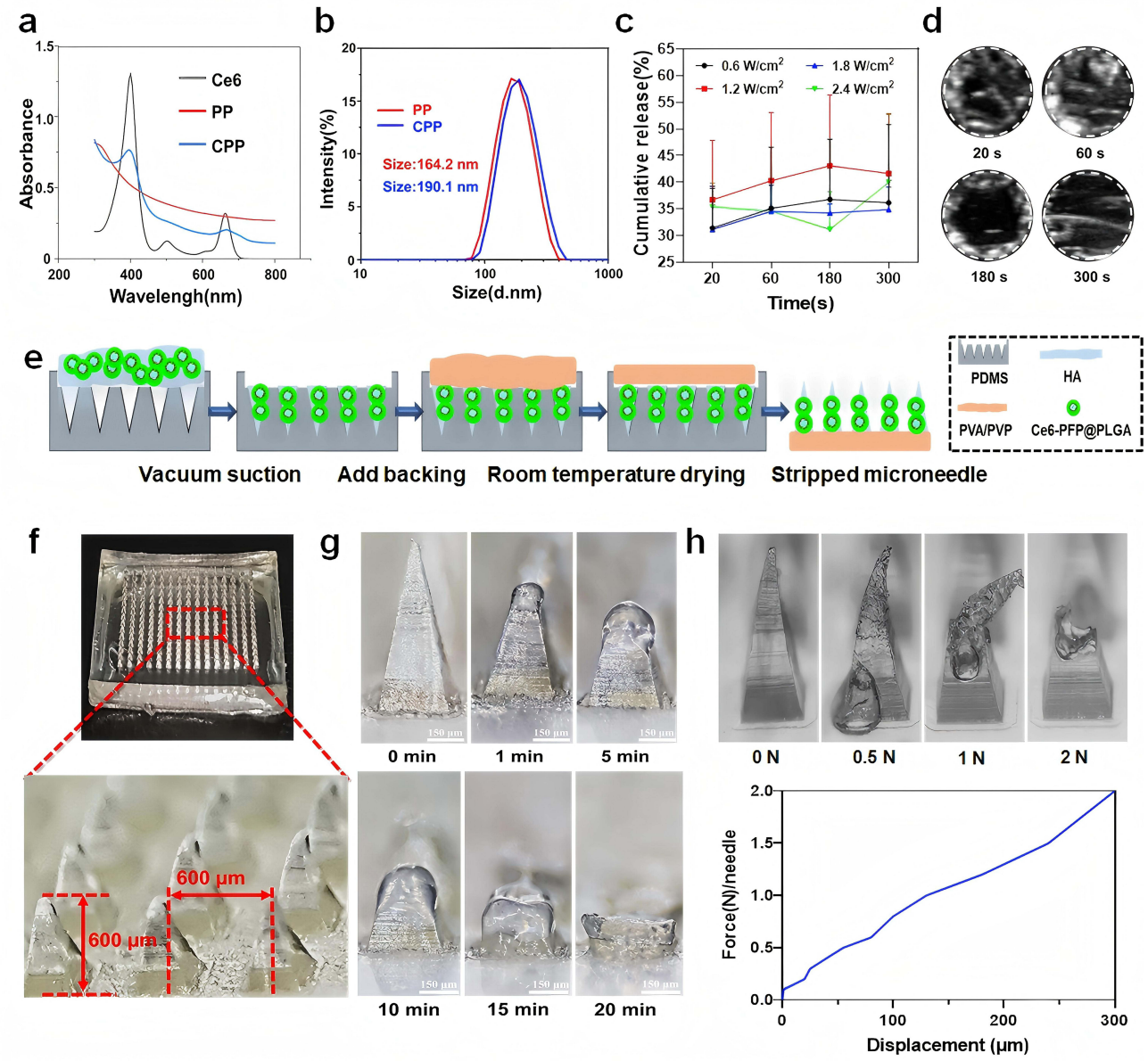

Figure 2 Preparation and characterization of CPP and CPP@MN. (**a**) UV-visible light absorption spectra of Ce6, PP, and CPP; (**b**) Comparison of particle size between PP and CPP; (**c**) In vitro drug release ability after CPP US irradiation; (**d**) US images of CPP irradiated using US irradiation (1 MHz, 1.2 W/cm^2) for different durations; (**e**) CPP@MN composite diagram; (**f**) CPP@MN surface morphology and stereoscopic observation; (**g**) CPP@MN diagram showing dissolution changes of needle tip at different times after isolated pig skin insertion (Scale bar: 150 μm); (**h**) Compression curve of the CPP@MNs and the corresponding optical microscopy images with different applied forces.

observed for the different irradiation durations. CPP echo intensity progressively increased during 0–5 min of US exposure, peaking at 1 min, followed by a sharp decline after post-3 min.

Based on the construction of the CPP, CPP@MN was established using the micromolding method, as shown in Figure 2e. The tips of the CPP@MN were arranged in a 15×15 mode, and the length between the adjacent tips and the tips of the CPP@MN was 600 μm (Figure 2f). CPP@MN was inserted into isolated pig skin and the height changes of the needle tip were recorded at different times. The results showed that CPP@MN dissolved significantly 1 min after insertion into isolated pig skin. The dissolution rate slowed until 20 min later, when the needle tip was completely dissolved, leaving only the base structure (Figure 2g).

A steady weight was applied to the tip of the needle to evaluate the mechanical strength of the CPP@MN. The results showed that with an increase in applied pressure, the needle tip gradually bent, and the compression distance of the

https://doi.org/10.2147/IJN.S537983

needle tip gradually increased until fracture occurred. The maximum mechanical pressure was able to withstand 2N (Figure 2h).

Evaluation of MN-Mediated Drug Delivery Enhancement Combined with Ultrasonic Cavitation in vitro

To visually evaluate the characteristics of the drug delivery mode of ultrasonic cavitation combined with microneedles under a stereomicroscope or fluorescence microscope, Evans Blue dye or DiO fluorescent dye was used as a model drug, and EPP@MN and DPP@MN were constructed, respectively (Figure 3a). The microneedle skin penetration capability verification experiment showed that after the EPP@MN was inserted into the isolated pig skin, orderly arranged blue micropores were observed in the central area of the isolated pig skin, and the distribution pattern was consistent with that

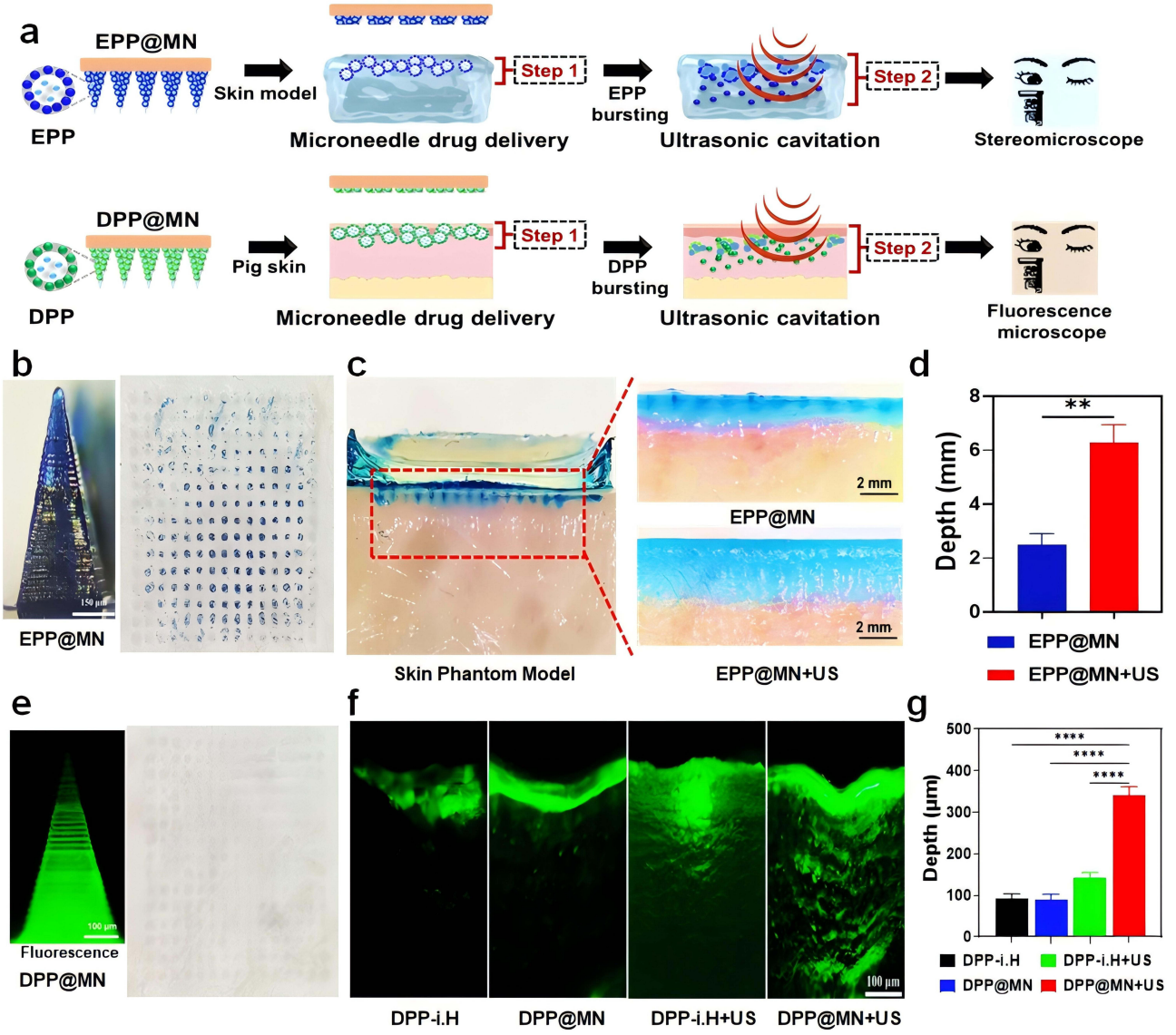

Figure 3 Penetrating capability of drug penetration in vitro. (**a**) Schematic diagram of microneedle drug delivery combined with ultrasonic cavitation to promote drug penetration; (**b**) EPP@MN microscopic view (Scale bar: 100 μm). The blue micromole in the 15×15 array indicates that EPP@MN successfully penetrated the isolated pig skin; (**c** and **d**) EPP@MN penetration depth and quantification of drug inserted into agarose skin phantom (Scale bar: 2 mm, n=3. **p < 0.005); (**e**) DPP@MN Structural fluorescence microscope image (Scale bar: 100 μm) and light microscope image after penetrating the isolated pig skin; (**f** and **g**). The penetration depth and quantification of drug fluorescence after DPP@MN insertion into isolated pig skin (Scale bar: 100 μm, n=3. ****p < 0.0001). All data above are presented as means ± SD.

of the EPP@MN array (Figure 3b). After EPP@MN was inserted into the agarose skin phantom and irradiation with US or without US, the results showed that, compared with the EPP@MN group, the penetration capacity of Evans Blue in the EPP@MN+US group was significantly enhanced, with deeper diffusion and wider distribution (Figure 3c). Quantitative analysis revealed that the penetration depth of Evans Blue in the EPP@MN group was 2.50 ± 0.40 mm. The penetration depth of Evans Blue in the EPP@MN+US group was 6.27 ± 0.68 mm, which is 2.5 times that of EPP@MN group (Figure 3d).

After DPP@MN was inserted into isolated pig skin and irradiated with or without US, fluorescence microscopic observation showed that the DPP@MN needle tip had a uniform green fluorescence distribution. The microneedle array entirely penetrated the isolated pig skin tissue (Figure 3e). DPP@MN was inserted into isolated pig skin to verify the function of the drug-promoting osmosis. Fluorescence microscopy revealed different degrees of DiO green fluorescence signal penetration in isolated pig skin of the four groups (Figure 3f). Quantitative analysis revealed the presence of DPP-i.H, DPP-i.H+US, DPP@MN and DPP@MN+US group, the DiO penetration depth was 92.78 ± 8.76 μm, 143.70 ± 8.56 μm, 88.15 ± 11.84 μm and 339.63 ± 17.46 μm, respectively. The penetration depth of DiO in the DPP@MN+US group was 3.85 times that in the DPP@MN group (Figure 3g).

Evaluation of MN-Mediated Drug Delivery Enhancement Combined with Ultrasonic Cavitation in vivo

In this study, B16F10 cells were used to construct a tumor-bearing mouse model. DPP@MN was inserted into the tumor site of mice for 2 min and immediately removed. The pinholes on the skin of the mice gradually shrank over time and nearly healed after 15 min, indicating their minimally invasive nature (Figure 4a and b). The effect of microneedle administration combined with ultrasonic cavitation on the penetration capability of drugs into living tumors was observed in the tumor model (Figure 4c). Subsequently, DPP@MN was inserted into the tumor in situ of B16F10 tumor-bearing mice and randomly divided into the DPP@MN+US (US: 1 MHz, 1.4 W/cm², 20% duty ratio, 5 min) and DPP@MN control (without US). After treatment, tumor tissues and frozen sections were obtained. Moreover, observation showed that the DPP@MN+US group showed a significantly enhanced DiO fluorescence signal distribution and a significantly extended range of fluorescence penetration was significantly extended (Figure 4d). Quantitative analysis showed that the dye diffusion depth of DiO in the DPP@MN group was 100.42 ± 17.62 μm and that in the DPP@MN+US group was 352.36 ± 20.40 μm, which was 3.51 times that in the DPP@MN group (Figure 4e).

Anti-Tumor Effects of CPP@MN in vitro and in vivo

The cellular uptake of CPP exhibited time-dependent characteristics: weak green fluorescence was observed after 2 hours of co-incubation. Fluorescence intensity peaked at 4 hours (Figure S1) and was maintained at 8 hours (indicating uptake saturation) CCK-8 assays demonstrated that after 4 hours of co-incubation with CPP without US irradiation – even at the highest concentration (32 μg/mL encapsulated Ce6) – cell viability remained unaffected, confirming CPP's biocompatibility. In contrast, US irradiation significantly reduced cell viability, indicating that CPP combined with US potently induces tumor cell death (Figure S2).

Intracellular ROS generation in CPP under US irradiation was investigated via fluorescence microscopy using DCFH-DA as a ROS fluorescent indicator. As shown in Figure 5a, the fluorescence intensity of the CPP+US group was the strongest, and SDT-mediated cytotoxicity (Figure 5b) demonstrated strong red fluorescence in the CPP+US and CPP@MN+US groups, predominant green fluorescence in the controls, and minimal red signals in the US/CPP/CPP@MN groups. The in vivo outcomes (Figure 5c and d) indicated delayed tumor progression in CPP@MN+US-treated mice (vs controls) with sustained growth suppression. Body weight remained stable across all groups (Figure 5e). Histologically, CPP@MN+US induced tumor tissue disintegration with pyknotic nuclei, reduced neovascularization (H&E staining), and reduced nuclear fragmentation with intense TUNEL staining (Figure 5f).

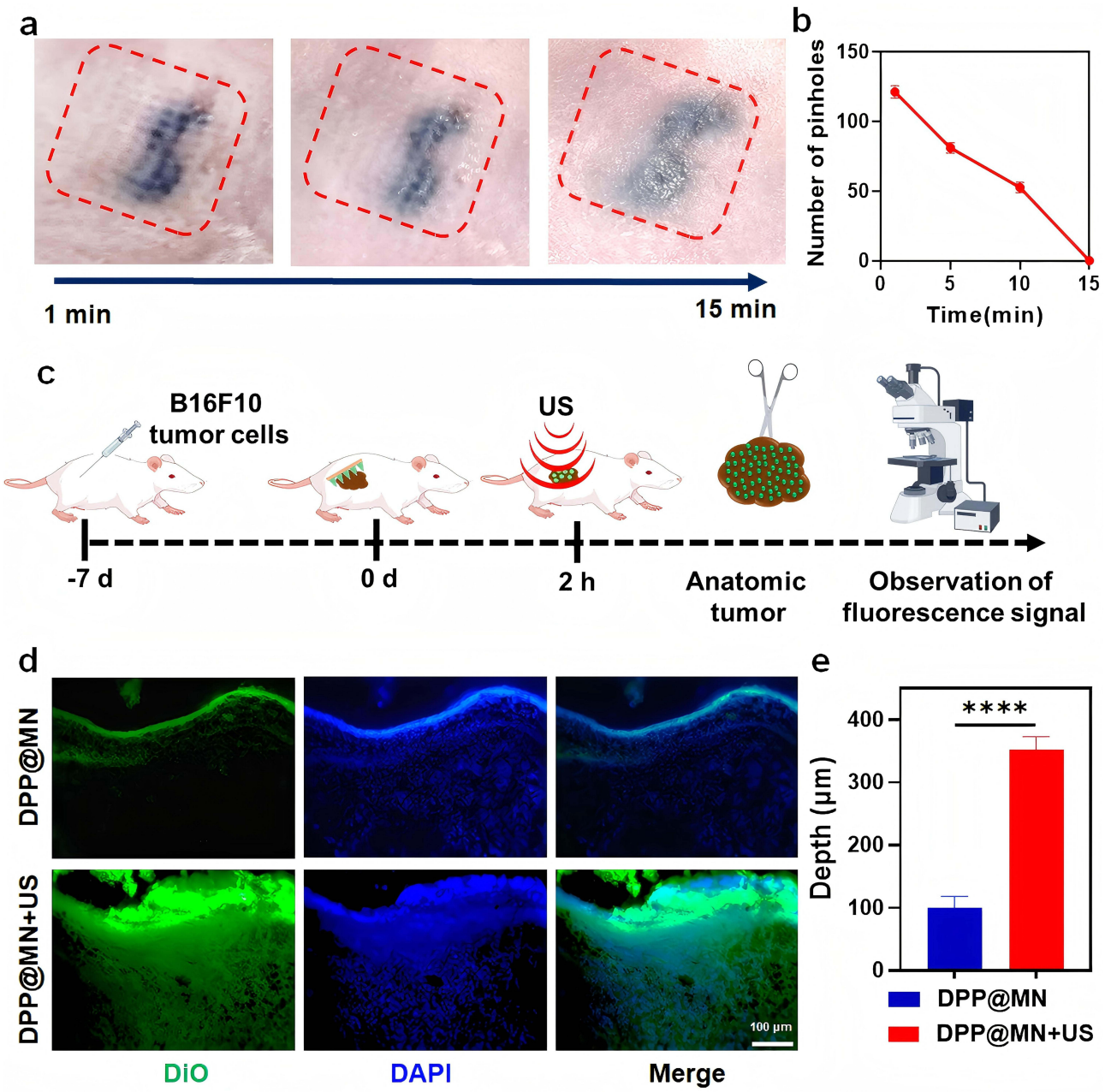

Figure 4 Tumor-penetrating capability drug penetration in vivo. (**a** and **b**) Changes of pinholes over time and pinhole count on the skin surface of mice after CPP@MN was inserted into the tumor site and removed immediately; (**c**) Microneedle drug delivery combined with ultrasonic cavitation mediates tumor infiltration; (**d** and **e**) DPP@MN was inserted into a mouse tumor-bearing model with ultrasound to promote drug penetration and quantitative analysis (Scale bar: 100 μm, n=3. ****p < 0.0001). All data above are presented as means ± SD.

Discussion

In this study, to address the problems of insufficient accumulation and limited penetration depth of sonosensitizers, CPP@MN, termed the "stepwise drug delivery" system, was established. With the combination of MN and the ultrasonic cavitation effect, it was proved that the penetration efficiency and diffusion rate were significantly enhanced by 4 times. This innovative drug delivery system not only overcomes the long-term challenges of insufficient aggregation and penetration capability of sonosensitizers in SDT, but also builds a multifunctional controllable drug release platform, providing an effective strategy to overcome biological barriers to improve therapeutic efficacy and avoids the need for complex nanoparticle modification, presenting a promising prospect for clinical translation.

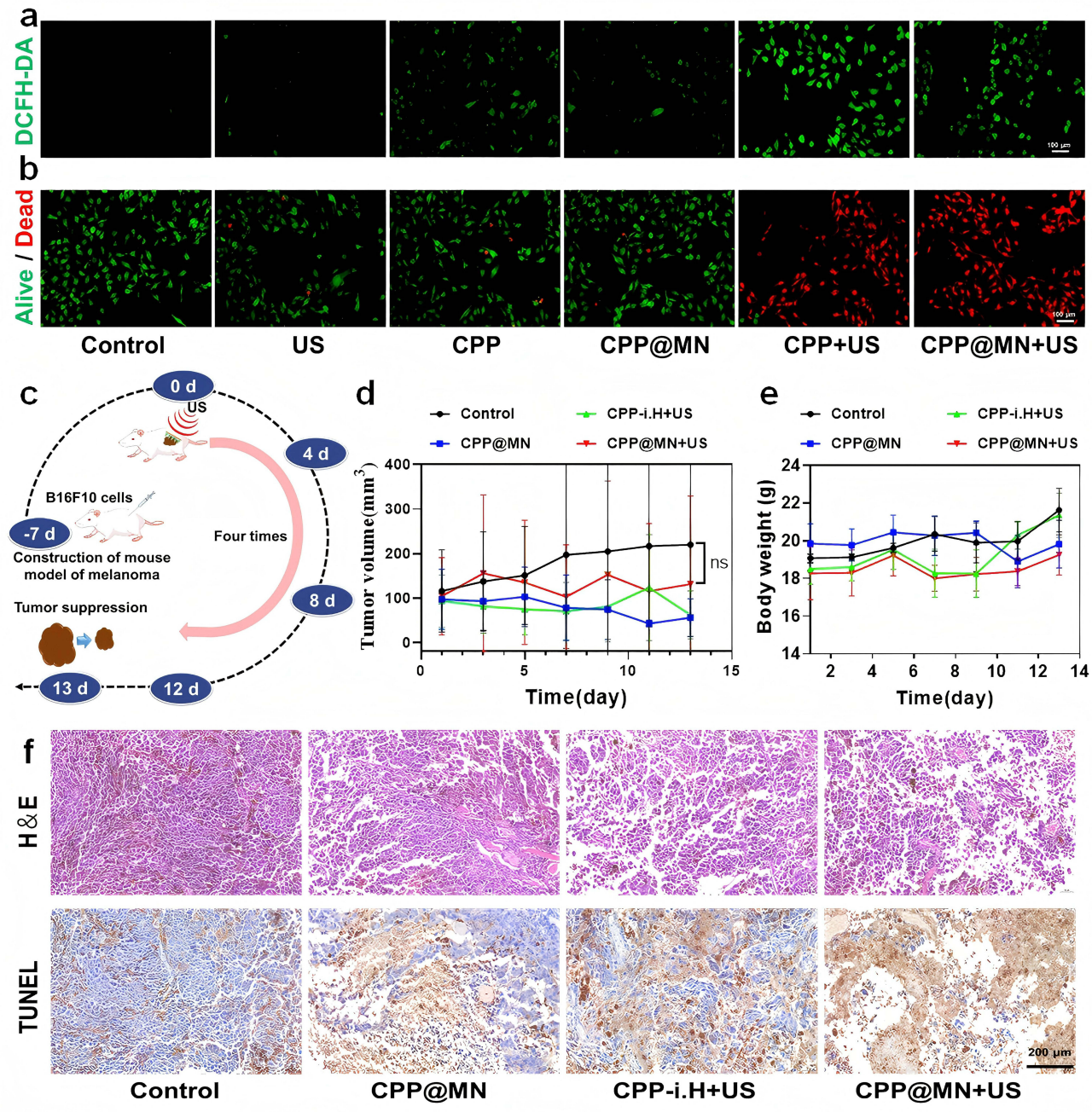

Figure 5 Evaluation of Anti-tumor effects of CPP@MN combined with ultrasonic cavitation. (**a**) ROS fluorescence images of different experimental groups (Scale bar: 100 μm); (**b**) Staining results of live/dead B16F10 cells in different experimental groups (Scale bar: 100 μm, green: live cells; Red: dead cells); (**c**) Schematic diagram of tumor inhibition experiment in B16F10 tumor-bearing mouse mo (**d**) Comparison of tumor volume and size between different experimental groups during treatment; (**e**) Weight change curves of mice in different experimental groups during treatment; (**f**) H&E and TUNEL staining of tumor tissues in different experimental groups.

In this system, the preparation of CPP@MN is the key link in this study to improve the efficiency of drug transdermal delivery. To realize the function of ultrasonic cavitation-mediated deep penetration of drugs, PLGA nanoparticles loaded with the sonosensitizer Ce6 and liquid-gas phase transition PFP were developed. PLGA, a polymer with good biocompatibility, has been approved by the FDA for clinical applications and is a widely used drug carrier.[26] As evidenced by multiple studies, nanoparticles with diameters below 200 nm are predominantly internalized via clathrin-mediated endocytosis, whereas phagocytosis becomes the dominant pathway for particles exceeding 500 nm.[27,28] The results showed that the particle size of CPP was 190.1 ± 4.2 nm, with the characteristics of uniformity and good stability, which could ensure that CPP could be obtained by cells (Figure 2a and b). The low boiling point of PFP enables US-

https://doi.org/10.2147/IJN.S537983

triggered liquid-to-gas phase transition, generating microbubbles that induce controlled drug release. It was demonstrated that nanoparticle carried PFP could achieve ideal anti-tumor efficiency through US mediated targeted delivery of chemical drugs[29] or excellent anti-bacterial infection effect through ultrasonic cavitation meditated biofilm barriers destruction.[30] In this study, CPP showed excellent US response performance, with the Ce6 release rate reaching 43.08 ± 10.85% under US irradiation. In addition, when the ultrasonic intensity exceeded 1.2 W/cm² and the duration was longer than 1 min, drug concentration in supernatant showed a downward trend, which may be related to sample loss caused by the ultrasonic cavitation effect.[29]

Skin, which formed a dense barrier for avoiding pathogen invasion, is the key interface between the body and the external environment.[31] However, it also limited the drugs with larger molecular weights, high polarity, and hydrophobicity to penetrate the basement membrane and reach the dermis.[7] Therefore, CPP@MN was synthesized through a two-step micro-molding approach.[23] The CPP@MN, whose distance between individual tip was 600 μm, could withstand a mechanical pressure of up to 2 N, much higher than the minimum force of 0.058 N required for penetrating human skin.[32] These results demonstrate that the CPP@MN used in this study is a viable transdermal nanoparticle delivery platform. Owing to the elasticity of the skin and rapid dissolution of the MNs matrix during insertion, it only reaches the dermis and does not penetrate the skin.[33]

To break the skin barrier and achieve deep penetration and accumulation of drugs at the tumor site, a "stepwise drug delivery" system was developed. To prove the function of deep penetration depth of sonosensitizers in tumor tissues mediated by CPP@MN combined with ultrasonic cavitation, delivery efficiency was evaluated in three different scenarios, including a 2.6% agarose skin phantom, whose viscoelastic characteristics are highly matched with pig ear tissue,[34] isolated pig skin, and in vivo tumor. As shown in Figures 3 and 4, the microneedles penetrated the agarose skin phantom and isolated the pig skin tissues; there was no significant deformation in the needle tip structure. When EPP@MN was inserted into the isolated pig skin, regular microchannels appeared in the central area of the tissue. However, incomplete local puncture was observed in the marginal area,[35] owing to uneven pressure distribution during the puncture procedure, regional variation in stratum corneum thickness, or mechanical transport characteristics of the microneedle array.

Furthermore, the distribution of Evans Blue on the agarose skin phantom, which was observed under stereomicroscopy, proved that the EPP@MN formed a blue channel consistent with the tip morphology when inserted. Gu et al developed a super-fast-acting microneedle patch (URA-MN) that uses effervescence to generate CO_2 bubbles to trigger drug release, achieving rapid penetration within 5 min in the delivery of macromolecules, such as liraglutide/insulin/heparin,[8] with the core advantage of minimally invasive intervention and rapid onset synergy. On a relative scale, the EPP@MN+US group exhibited 2.5 times (Figure 3b–d) greater Evans Blue penetration depth vs EPP@MN alone (in vitro agarose skin phantom), while DPP@MN+US achieved 3.85 times (ex vivo porcine skin) and 3.51 times (in vivo tumors) enhanced DiO permeation compared to DPP@MN (Figures 3e–g and Figure 4d and e), demonstrating that the synergistic effect of microneedles and ultrasound can significantly enhance drug penetration efficiency. These results align with previous findings using PFH-PLGA-NH_2 nanobubbles, which achieved 728 μm drug penetration depth in porcine skin models.[7] Notably, multi-array MN patches enable decentralized drug delivery (vs single-point injection), increasing tumor-site drug aggregation.[36] Consistently, the results of this study show that the depth of DiO penetration in the DPP@MN+US group was 195.93μm higher than that in the i.H+US group (Figure 3f), which was consistent with the trend reported in the literature.

Reactive oxygen species (ROS) serve as terminal effector molecules in sonodynamic therapy-mediated anti-tumor effects.[35] The results of ROS detection showed that the CPP@MN combined with US irradiation significantly promotes ROS production. Double staining of live/dead cells showed that cell mortality in the CPP@MN+US group was consistent with that in the CPP+US group. The results showed that Ce6-encapsulated nanomedicine enhanced the killing ability of SDT[37] and further demonstrated that microneedle encapsulation of nanoparticles did not affect their SDT effect. Using melanoma sonodynamic therapy (SDT) as a representative application model, B16F10 tumor-bearing mice were established and the anti-tumor efficiency of "stepwise drug delivery" system was further evaluated. The findings indicated that, following a 13-day treatment period, as opposed to the control group, the tumor volume in the CPP@MN+US group exhibited a significantly slower growth rate, thereby demonstrating a distinct inhibitory effect

on tumor proliferation. H&E and TUNEL staining analyses of mouse tumors indicated that the CPP@MN+US group had specific anti-tumor effects. In this study, CPP@MN was prepared using HA as a needle-tip material. Although the preparation process is simple and the stability is good, the material limits the drug-loading capacity, resulting in insignificant tumor suppression. Moreover, the drug release rate mainly depends on the dissolution of the material and is difficult to precisely control. Further improvements are required to meet the therapeutic requirements for specific release rates. In addition, in in vivo experiments, the in situ tumors have irregular shapes, mainly protruding spherical shapes. This increases the difficulty of microneedles being completely inserted into the local skin of the cancer and covering the lesion area, which is also why the treatment effect is not apparent. In subsequent research, the skin insertion ability of microneedles will be optimized.

Conclusion

In this study, based on the application scenario of SDT for malignant superficial tumors; to enhance the tumor-penetrating capability of sonosensitizers at the tumor site, we build a "stepwise drug delivery" system integrating dissolvable microneedles (CPP@MN) with US-responsive nanoparticles. The results showed that CPP@MN has excellent skin penetration capability, solubility, and mechanical strength. Drug penetration experiments on three experimental models (in vitro agarose skin phantom, ex vivo pig skin, and in vivo tumors) confirmed that compared with simple microneedles and local injection, microneedle administration combined with ultrasonic cavitation could deliver drugs evenly and deeply to the tumor site. This drug delivery system not only significantly promotes deep penetration of sonosensitizer in SDT, but also provides an efficient drug delivery mode for superficial tumor treatment.

Abbreviations

SDT, sonodynamic therapy; MN, microneedle; CPP, Ce6-PFP@PLGA; PFP, perfluoropentane; Ce6, chlorin e6; US, ultrasound; TDDS, transdermal drug delivery system; HA, hyaluronic acid; PP, PFP@PLGA; DPP, De6-PFP@PLGA; EPP: Ee6-PFP@PLGA.

Acknowledgments

This work was supported by the National Natural Science Foundation of China (82272028) and Hunan Provincial Health High-Level Talent Scientific Research Project (R2023010).

Disclosure

The author(s) report no conflicts of interest in this work.

References

1. Wang M, Li X, Du W, et al. Microneedle-mediated treatment for superficial tumors by combining multiple strategies. *Drug Deliv Transl Res*. 2023;13(6):1600–1620. doi:10.1007/s13346-023-01297-9
2. Zheng Y, Wang W, Gao Y, et al. Nanosonosensitizers-engineered injectable thermogel for augmented chemo-sonodynamic therapy of melanoma and infected wound healing. *Mater Today Bio*. 2023;20:100621. doi:10.1016/j.mtbio.2023.100621
3. Yan P, Liu LH, Wang P. Sonodynamic therapy (SDT) for cancer treatment: advanced sensitizers by ultrasound activation to injury tumor. *ACS Appl Bio Mat*. 2020;3(6):3456–3475. doi:10.1021/acsabm.0c00156
4. McEwan C, Nesbitt H, Nicholas D, et al. Comparing the efficacy of photodynamic and sonodynamic therapy in non-melanoma and melanoma skin cancer. *Bioorg Med Chem*. 2016;24(13):3023–3028. doi:10.1016/j.bmc.2016.05.015
5. Hu C, Hou B, Xie S. Application of nanosonosensitizer materials in cancer sono-dynamic therapy. *RSC Adv*. 2022;12(35):22722–22747. doi:10.1039/d2ra03786f
6. Lammers T. Nanomedicine tumor targeting. *Adv Mat*. 2024;36(26):e2312169. doi:10.1002/adma.202312169
7. Han X, Wang F, Shen J, et al. Ultrasound nanobubble coupling agent for effective noninvasive deep-layer drug delivery. *Adv Mat*. 2024;36(3):e2306993. doi:10.1002/adma.202306993
8. Subramanian AK, Thayalan D, Edwards AI, et al. Biomedical waste management in dental practice and its significant environmental impact: a perspective. *Env Technol Innov*. 2021;24:101807. doi:10.1016/j.eti.2021.101807
9. Zhang W, Jiao Y, Zhang Z, et al. Transdermal gene delivery. *J Controlled Release*. 2024;371:516–529. doi:10.1016/j.jconrel.2024.06.013
10. Carter P, Narasimhan B, Wang Q. Biocompatible nanoparticles and vesicular systems in transdermal drug delivery for various skin diseases. *Int J Pharmaceut*. 2019;555:49–62. doi:10.1016/j.ijpharm.2018.11.032
11. Zhi D, Yang T, Zhang T, et al. Microneedles for gene and drug delivery in skin cancer therapy. *J Controlled Release*. 2021;335:158–177. doi:10.1016/j.jconrel.2021.05.009

12. Sang M, Cho M, Lim S, et al. Fluorescent-based biodegradable microneedle sensor array for tether-free continuous glucose monitoring with smartphone application. *Sci Adv*. 2023;9(22):eadh1765. doi:10.1126/sciadv.adh1765
13. Phatale V, Vaiphei KK, Jha S, et al. Overcoming skin barriers through advanced transdermal drug delivery approaches. *J Controlled Release*. 2022;351:361–380. doi:10.1016/j.jconrel.2022.09.025
14. Li J, Wang X, Wang Z, et al. A transdermal drug delivery system based on dissolving microneedles for boron neutron capture therapy of melanoma. *Biomat Sci*. 2023;11(23):7568–7578. doi:10.1039/d3bm01262j
15. Zheng B, Li Q, Fang L, et al. Microorganism microneedle micro-engine depth drug delivery. *Nat Commun*. 2024;15(1):8947. doi:10.1038/s41467-024-53280-8
16. Su Y, Yang F, Wang M, Cheung PCK. Cancer immunotherapeutic effect of carboxymethylated β-d-glucan coupled with iron oxide nanoparticles via reprogramming tumor-associated macrophages. *Int J Biol Macromol*. 2023;228:692–705. doi:10.1016/j.ijbiomac.2022.12.154
17. Du M, Wang T, Peng W, et al. Bacteria-driven nanosonosensitizer delivery system for enhanced breast cancer treatment through sonodynamic therapy-induced immunogenic cell death. *J Nanobiotechnol*. 2024;22(1):167. doi:10.1186/s12951-024-02437-0
18. Zhang C, Chen S, Li Q, et al. Ultrasound-targeted microbubble destruction mediates gene transfection for beta-cell regeneration and glucose regulation. *Small*. 2021;17(31):e2008177. doi:10.1002/smll.202008177
19. Chen Y, Du M, Yuan Z, et al. Spatiotemporal control of engineered bacteria to express interferon-γ by focused ultrasound for tumor immunotherapy. *Nat Commun*. 2022;13(1):4468. doi:10.1038/s41467-022-31932-x
20. Yu Y, Tan L, Li Z, et al. Single-atom catalysis for efficient sonodynamic therapy of methicillin-resistant staphylococcus aureus-infected osteomyelitis. *ACS Nano*. 2021;15(6):10628–10639. doi:10.1021/acsnano.1c03424
21. Xin L, Shen JX, Huang ZX, et al. Ultrasound-launched targeted nanoparticle enhances antibacterial sonodynamic therapy for effective eradication of pseudomonas aeruginosa biofilm. *BIO Integration*. 2024;5(1):1–15. doi:10.15212/bioi-2024-0001
22. Xu J, Cai H, Wu Z, et al. Acoustic metamaterials-driven transdermal drug delivery for rapid and on-demand management of acute disease. *Nat Commun*. 2023;14(1):869. doi:10.1038/s41467-023-36581-2
23. Feng W, Liu Z, Xia L, et al. A sonication-activated valence-variable sono-sensitizer/catalyst for autography inhibition/ferroptosis-induced tumor nanotherapy. *Angewandte Chemie*. 2022;61(48):e202212021. doi:10.1002/anie.202212021
24. Qu F, Wang P, Zhang K, et al. Manipulation of mitophagy by "All-in-One" nanosensitizer augments sonodynamic glioma therapy. *Autophagy Vol*. 2020;16(8):1413–1435. doi:10.1080/15548627.2019.1687210
25. Liao S, Cai M, Zhu R, et al. Antitumor effect of photodynamic therapy/sonodynamic therapy/sono-photodynamic therapy of chlorin e6 and other applications. *Mol Pharm*. 2023;20(2):875–885. doi:10.1021/acs.molpharmaceut.2c00824
26. Peng J, Zhou J, Sun R, et al. Dual-targeting of artesunate and chloroquine to tumor cells and tumor-associated macrophages by a biomimetic PLGA nanoparticle for colorectal cancer treatment. *Int J Biol Macromol*. 2023;244:125163. doi:10.1016/j.ijbiomac.2023.125163
27. Zhou Q, Liu Q, Wang Y, et al. Bridging smart nanosystems with clinically relevant models and advanced imaging for precision drug delivery. *Adv Sci*. 2024;11(14):e2308659. doi:10.1002/advs.202308659
28. He SS, Fu YN, Tan ZC, et al. Optimization of ultra-small nanoparticles for enhanced drug delivery. *BIO Integ*. 2023;4(2):62–69. doi:10.15212/bioi-2022-0015
29. Du M, Wang T, Feng R, et al. Establishment of ultrasound-responsive SonoBacteriaBot for targeted drug delivery and controlled release. *Front Bioeng Biotechnol*. 2023;11:1144963. doi:10.3389/fbioe.2023.1144963
30. Xin L, Zhang C, Chen J, et al. Ultrasound-activatable phase-shift nanoparticle as a targeting antibacterial agent for efficient eradication of pseudomonas aeruginosa biofilms. *ACS Appl Mat Interf*. 2022;14(42):47420–47431. doi:10.1021/acsami.2c13166
31. Han W, Liu F, Muhammad M, et al. Application of biomacromolecule-based passive penetration enhancement technique in superficial tumor therapy: a review. *Int J Biol Macromol*. 2024;272(Pt 1):132745. doi:10.1016/j.ijbiomac.2024.132745
32. You J, Yang C, Han J, et al. Ultrarapid-acting microneedles for immediate delivery of biotherapeutics. *Adv Mat*. 2023;35(45):e2304582. doi:10.1002/adma.202304582
33. Liu F, Cheng Z, Yi H. NIR light-activatable dissolving microneedle system for melanoma ablation enabled by a combination of ROS-responsive chemotherapy and phototherapy. *J Nanobiotechnol*. 2023;21(1):61. doi:10.1186/s12951-023-01815-4
34. Zhang D, Das DB, Rielly CD. Microneedle assisted micro-particle delivery from gene guns: experiments using skin-mimicking agarose gel. *J Pharmaceut Sci*. 2014;103(2):613–627. doi:10.1002/jps.23835
35. Liang M, Shang L, Yu Y, et al. Ultrasound activatable microneedles for bilaterally augmented sono-chemodynamic and sonothermal antibacterial therapy. *Acta Biomat*. 2023;158:811–826. doi:10.1016/j.actbio.2022.12.041
36. Huang S, Wen T, Wang J, et al. Nanoparticle-integrated dissolving microneedles for the co-delivery of R848/aPD-1 to synergistically reverse the immunosuppressive microenvironment of triple-negative breast cancer. *Acta biomat*. 2024;176:344–355. doi:10.1016/j.actbio.2024.01.009
37. Huang S, Ding D, Lan T, et al. Multifunctional nanodrug performs sonodynamic therapy and inhibits TGF-β to boost immune response against colorectal cancer and liver metastasis. *Acta biomat*. 2023;164:538–552. doi:10.1016/j.actbio.2023.04.001